Spectroscopic Studies of Catanionic Reverse Microemulsion: Correlation with the Superactivity of Horseradish Peroxidase Enzyme in a Restricted Environment

Ranjit Biswas,*,† Arup R. Das,† Tuhin Pradhan,† Didier Touraud,‡ Werner Kunz,*,‡ and Sekh Mahiuddin*,§

Department of Chemical, Biological and Macromolecular Sciences, and Unit for Nanoscience and Technology, S. N. Bose National Centre for Basic Sciences, JD Block, Sector III, Salt Lake City, Kolkata 700 098, India, Institute of Physical and Theoretical Chemistry, University of Regensburg, D-93040 Regensburg, Germany, and Material Science Division, North−East Institute of Science and Technology, Jorhat 785006, Assam, India

Received: December 2, 2007; Revised Manuscript Received: February 29, 2008

Catanionic microemulsions formed by dodecyltrimethylammonium bromide (DTAB), sodium dodecyl sulfate (SDS), *n*-hexanol, dodecane, and citrate buffer have been characterized by using dynamic light scattering (DLS) and spectroscopic studies. While the DLS measurements provide information about the hydrodynamic diameters of the microemulsion droplets formed upon variation of the constituents, steady-state and time-resolved fluorescence emission experiments probe the polarity and the dynamics of the trapped solvent pool inside of the microemulsion droplets of nanometer dimension. In addition, time-resolved fluorescence anisotropy shows the rigidity of the confined solvent pool as well as the coupling between the motion of a solute and those of the solvent molecules. The results obtained from the DLS and those from the steady-state and time-resolved fluorescence emission studies have been found to correlate well with the superactivity of horseradish peroxidase enzyme in the catanionic microemulsions. Subsequently, the time-zero estimate for the dynamic Stokes shift in these microemulsions reveals that approximately 50% of the total solvent dynamical response is missed due to the limited time resolution employed in our experiments. The amplitude of the missing portion is similar to what has been observed recently for nanoscopic water by Fayer and co-workers (Piletic, I. R.; Tan, H.-S.; Fayer, M. D. *J. Phys. Chem. B* 2005, *109*, 21273).

1. Introduction

A reverse microemulsion, which is a thermodynamically stable liquid, containing surfactant(s), cosurfactant, oil, and water typifies a biological model of a living cell.[1] In this system, water molecules are confined in a reaction vessel of nanometer dimension, dispersed in a continuous oil medium. A water-in-oil reverse microemulsion is an example of such a system. The behavior of water molecules inside of the pool is similar in many aspects to water molecules bound to biological systems and in other restricted environments.[1–34]

In order to understand the behavior of water inside the pool in a reverse microemulsion, where many chemical and physiochemical processes can occur, solvation and rotational dynamics have been studied using different techniques.[20–29] The solvent relaxation times in a water pool of a microemulsion are found to be many times slower than those in bulk water.[1–3,6–10] The size of the water pool can be tailor-made by controlling the water to surfactant ratio for making microemulsions mimic a biological system or any other restricted environment. Literature shows that reverse microemulsions containing sodium bis(2-ethylhexyl) sulfosuccinate (aerosol-OT or commonly AOT), an anionic amphiphile, have frequently been taken as a biological model, in contrast to cationic or mixed amphiphiles.[1–3] However, a biological system contains not only anionic or uncharged components but also positively charged molecules. Therefore, catanionic reverse microemulsions appear to be a better model for many biological systems.[34]

A catanionic reverse microemulsion as a reaction medium is rarely used,[34–38] except for solubilization and phase behavior studies.[39–43] The first example for the enzyme activity in a catanionic reverse microemulsion appeared in 2005 and demonstrated that at a certain composition of sodium dodecyl sulfate (SDS) and dodecyltrimethylammonium bromide (DTAB), this catanionic microemulsion exhibits enzymatic superactivity[34] at a DTAB to total surfactant ratio of 15%, even though DTAB has a negative effect on enzymes.[44] Interestingly, the enzymatic activity in this catanionic microemulsion is up to a DTAB mole fraction of 0.15, in comparison to microemulsions containing only SDS as the surfactant.[45] All of these results are somewhat surprising since DTAB even at $\leq 10^{-2}$ M strongly inhibits the enzyme activity.[44] The cosurfactant (*n*-hexanol) also has negative effect on the enzymatic activity, which is probably due to the denaturation of the enzyme structure by the alcohol.[46,47] Therefore, the superactivity of the enzyme might be related to a just optimum level of hydration, which is supplied by the finite-sized water pool confined in this reverse microemulsion. It seems that DTAB resides at the oil−water interface and therefore minimizes the poisoning of the enzyme due to limited contact. Another reason for the superactivity of the enzyme could be that the pH inside the droplets of the SDS/DTAB microemulsions is close to the critical value of 4.5, at which the initial velocity of the enzymatic activity is maximum. Note that the pure buffer has a pH value of 5.[34]

Recently, several experimental,[48–50] computer simulation,[51,52] and theoretical studies[53–55] have indicated the role of structure and dynamics of water molecules near a biological surface in

* To whom correspondence should be addressed. E-mail: ranjit@bose.res.in (R.B.); werner.kunz@chemie.uniregensburg.de (W.K.); mahirrljt@yahoo.com (S.M.).

† S. N. Bose National Centre for Basic Sciences.

‡ University of Regensburg.

§ North−East Institute of Science and Technology.

10.1021/jp711368p CCC: $40.75
Published on Web 05/06/2008

determining the functional activity of that moiety. Very recently, Abecassis et al.[56] have studied the microstructure and phase behavior of a "true" catanionic reverse microemulsion and concluded that the surface charge of a catanionic microemulsion plays a significant role in the microstructure, which can be tailor-made. In fact, there has been a great deal of interest in correlating the function of protein molecules with the dynamics of the water molecules surrounding it.[48–50] Since the three-dimensional hydrogen bonding network structure of water molecules near to a biologically active site and those in a confinement are expected to be strongly modified, both the polarity and dynamics of these molecules are likely to be very different from those in the bulk. In addition, the hydration layers surrounding an active site or a dipolar probe in a finite size confinement are microscopically heterogeneous (both structurally and dynamically) due to binding via electrostatic and other specific interactions.[1–3,6–16] These interactions render the water dynamics much slower but cannot make them too sluggish to stop the functional activity of that particular protein or enzyme. The role of this heterogeneity and dynamics in keeping a protein or enzyme functional is an aspect of constant debate and discussion. As the polarity of the water molecules trapped in a confinement is very different, a reaction is also likely to be affected.

In this Article, we are studying the average polarity and dynamics of the confined solvent pool inside catanionic reverse microemulsions formed by mixing five components, SDS, DTAB, dodecane, *n*-hexanol, and water (present as a buffer). Various components of this mixture are varied in order to change the size of the droplets formed. The hydrodynamic diameters of these reverse microemulsion droplets have been determined by using the DLS technique. The average polarity and the dynamics of the confined solvent pool inside these droplets have been probed via steady-state and time-resolved fluorescence emission spectroscopy. Anisotropy studies have been carried out to gain a qualitative idea about the rigidity of the confined solvent pool. Subsequently, an attempt has been made to correlate the DLS and spectroscopic results with the enzymatic activity of horseradish peroxidase[57] obtained earlier in these reverse microemulsions.[34]

The organization of the rest of the paper is as follows. Experimental details including materials, experimental techniques and analyses methods have been described briefly in the next section. Section 3 contains the Results and Discussion. The paper then ends with concluding remarks in section 4.

2. Experimental Section

2.1. Materials. Sodium dodecyl sulfate (≥99%, SRL, India), dodecyltrimethylammonium bromide (>99%, Aldrich, Germany), *n*-hexanol (>98%, Acros Organics, U.S.A.), and *n*-dodecane (>99%, Aldrich, Germany) were used without further purification. A buffer of pH 5 consisting of 0.009 mol L^{-1} citric acid monohydrate (99.5%, Qualigens, India) and 0.016 mol L^{-1} sodium citrate dihydrate (>99%, BDH, India) were used for preparation of microemulsion and maintaining pH. Double-distilled water was used to prepare the solutions.

2.2. Preparation of Microemulsion. We have three series of catanionic microemulsions. In the first series, DTAB was varied (1.576, 2.222, 2.828, and 3.434%) by keeping the total surfactant (SDS + DTAB) composition at 20.2%, the cosurfactant (*n*-hexanol) at 20.2%, *n*-dodecane at 37.6%, and the buffer at 22%. Under this series, the microemulsions are designated as ME10, ME11, ME12, and ME13, respectively. In the second series of microemulsions, the composition of *n*-hexanol was varied (20.2, 22, 25, 28.9, and 30%) taking the composition of ME10 as the base value, and the total composition of *n*-hexanol and *n*-dodecane was kept at 57.8%. The micoemulsions were designated as ME10, ME14, ME15, ME16, and ME17. In the third series, the buffer composition was varied (22, 20, 18, 15, and 10%), keeping the total composition of the buffer and *n*-dodecane at 59.6%, and the microemulsions were designated as ME10, ME18, ME19, ME20, and ME21. The composition of different components was in % w/w with respect to the total microemulsion composition. In all three series of microemulsions, ME10 was common. Addition of calculated amounts of the components followed by stirring produced the samples, which were transparent to the bare eyes. Table 1 summarizes the sample (catanionic reverse microemulsions) composition.

TABLE 1: Compositions of Microemulsions (ME) (numbers are the code numbers starting from ME10 to ME21)

(a) Variation of SDS to DTAB Ratio for a Total Surfactant Content of 22.2%.

Sl no.	code No	weight fraction of SDS (=SDS/(SDS + DTAB)
1	ME13	0.830
2	ME12	0.860
3	ME11	0.890
4	ME10	0.9221

(b) Variation of Hexanol to Dodecane Ratio for a Total Composition (Hexane + Dodecane) of 57.8%

Sl no.	code no.	*n*-hexanol w/w %
1	ME10	20.20
2	ME14	22.00
3	ME15	25.00
4	ME16	28.90
5	ME17	30.00

(c) Variation of Buffer to Dodecane Ratio for a Total Content (Buffer + Dodecane) of 59.6%.

Sl no.	code no.	buffer w/w %
1	ME21	10.00
2	ME20	15.00
3	ME19	18.00
4	ME18	20.00
5	ME10	22.00

2.3. Spectroscopic Experiments. In a typical steady-state absorption and emission run, coumarin 153 (C153) was added to a microemulsion (concentration < 10^{-5} M), and the spectra were recorded with an UV−visible spectrophotometer (UV-2450, Shimadzu). An optically clean quartz cell with 1 cm optical path length was used for recording the spectra. Subsequently, the absorbance of the samples was adjusted (via dilution) to ~0.10, and emission spectra were collected with a Fluoromax-3, Jobin-Yvon fluorimeter. For each emission scan, the peak wavelength of the corresponding absorption spectrum was used as an excitation wavelength. Absorption and emission peak frequencies were calculated as an average of the peak frequencies obtained by fitting the upper half of the spectrum (absorption or emission) with an inverted parabola, the first moment, and the arithmetic mean of the frequencies at half intensities on both the blue and red ends of the spectrum.[58,59] This averaging takes care of the asymmetric movement of the spectral band as the sample composition changes.

The solvation dynamics in these media was followed by monitoring the peak shift in the time-resolved emission spectrum (TRES) of an excited probe (C153 in this case) constructed from

a series of 18−22 emission decays at equally spaced wavelengths across the steady-state emission spectrum of the dissolved probe.[60] The decays (magic angle) were collected via the time-correlated single-photon counting (TCSPC) method by using 409 nm light for excitation. The excitation wavelength (409 nm) for the time-resolved emission studies was kept fixed for all of the samples. The full width at half-maximum (fwhm) of the instrument response function (IRF) with this excitation source was approximately 75 ps. The collected decays were deconvoluted from the IRF and fitted to a multiexponential function using an iterative reconvolution algorithm. Such fitting enables one to capture relaxation processes with time scales in the range of ~15 ps. Note that this resolution might miss the relatively faster component of the solvent response but is expected to capture the long time dynamics well. Subsequently, the time-dependent progress of solvation was expressed in terms of the solvent response function,[60] $S(t) = [\nu(t) - \nu(\infty)]/[\nu(0) - \nu(\infty)]$, where $\nu(t)$ denotes the peak frequency of the emission spectrum at a certain time (t) after the laser excitation of the probe and $\nu(0)$ represents the emission peak frequency immediately after excitation (with the same environment configuration as that in the ground state).[60] The $\nu(\infty)$ is the peak frequency of the emission spectrum of the excited probe at a sufficiently long time when the reorganization of the environment is supposed to be completed. Therefore, $\nu(\infty)$ should be equal to the peak frequency of the steady-state emission spectrum of the same probe. Even though this would be the case for most of the solvents at ambient conditions and at higher temperatures, $\nu(\infty)$ might differ (by at most 300 cm^{-1}) from the steady-state value in systems where lowering the temperature or geometric confinement slows down the solvent motions substantially.[60] The average solvation time, $\langle\tau_s\rangle$, was determined from $S(t)$ as follows

$$\langle\tau_s\rangle = \int_0^\infty dt S(t)$$

Subsequently, the missing component of the fast initial decay of $S(t)$ was determined by estimating the time-zero spectrum[61] from the following relation,[29,62] $\nu_{em}(t=0) \approx \nu_{abs} - [\nu_{abs} - \nu_{em}]^{nonpolar}$. Here, ν_{abs} is the absorption peak frequency of C153 in a given microemulsion. The absorption and emission peak frequencies of C153 in nonpolar medium were taken as those obtained for C153 in heptane. In principle, these values should be obtained from the hypothetical microemulsion where nonpolar solvent alone constitutes the encapsulated solvent pool.

Emission decays for time-resolved anisotropy studies were collected at the peak wavelength of the steady-state emission bands so that the effects of fast decay or rise due to solvent reorganization were minimized. For a few cases, emission decays were collected at two or three different wavelengths around the peak of the emission band, and the analyzed data were found to vary within a small uncertainty. Time-resolved fluorescence anisotropies, $r(t)$, were calculated from the collected parallel ($I_{||}(t)$) and perpendicular ($I_{\perp}(t)$) decays by using the following well-known relation[63]

$$r(t) = \frac{I_{||}(t) - GI_{\perp}(t)}{I_{||}(t) + 2GI_{\perp}(t)} \quad (1)$$

where G accounts for the differential sensitivity to the two polarizations, which was obtained by tail matching the background-corrected intensity decays $I_{||}(t)$ and $I_{\perp}(t)$. The average value for G obtained by tail matching the relevant decays at times longer than the anticipated rotation time is 1.15 ± 0.05.

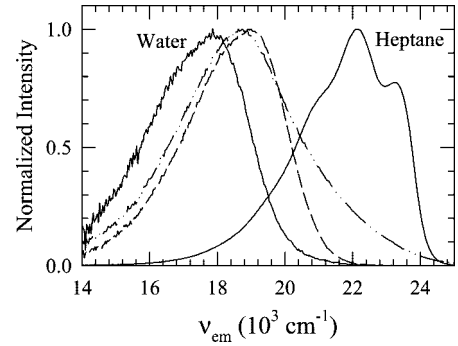

Figure 1. Emission spectra of C153 in water (solid line), microemulsion at 0.830 weight fraction of SDS content (dash−dot−dot line), hexanol (dashed line), and heptane (solid line). Note that the emission spectra in water and heptane are marked in the figure by "water" and "heptane", respectively. All emission spectra were obtained after exciting at 409 nm.

The time-resolved anisotropy constructed from the collected emission decays by using eq 1 was then fitted to a biexponential function after deconvoluting from the IRF using an iterative reconvolution-fitting program. The following form of the biexponential function was used for this purpose[63]

$$r(t) = r(0)[a_1 \exp(-t/\tau_1) + (1 - a_1)\exp(-t/\tau_2)] \quad (2)$$

where τ_1 and τ_2 in eq 2 represent the time constants associated with the decays of the components (a_i, $i = 1$ or 2) constituting $r(t)$. The $r(0)$ denotes the initial anisotropy and was taken as 0.376 for fitting the time-resolved anisotropies of C153 in all of the mixtures studied here.[63] The average rotational correlation time is determined as $\langle\tau_r\rangle = a_1\tau_1 + (1 - a_1)\tau_2$, which comes from the time integration of eq 2 after normalizing with $r(0)$.

2.4. DLS Experiment. The hydrodynamic diameters of the microemulsion droplets of different compositions were measured by using the dynamic light scattering (DLS) technique and by employing a 4 mW He−Ne laser (Nano S, Malvern, France) equipped with a thermostatted sample chamber. The scattering intensity data were processed (using the software supplied with the instrument) to obtain the hydrodynamic diameter (R_h). The hydrodynamic diameter (R_h) of the microemulsion droplets is estimated from the intensity autocorrelation function by using the relation $R_h = (k_BT)/(3\pi\eta D)$, where k_BT denotes, as usual, the Boltzmann constant (k_B) times the absolute temperature (T) and η is the medium viscosity. D is the translational diffusion coefficient of the droplet, which was determined from the intensity autocorrelation data.

3. Results and Discussion

3.1. Distribution of C153 in a Microemulsion. As mentioned in the Experimental Section, the systems considered in this study contain five major components, SDS/DTAB/*n*-hexanol/buffer/*n*-dodecane. Since these systems (microemulsion) are microscopically heterogeneous, the probe molecule (C153) is likely to be distributed among the components constituting the microemulsion at a given composition, which will induce an excitation wavelength dependence of the emission spectrum of C153. Figure 1 shows the emission spectra of C153 in water, *n*-hexanol and heptane along with the one in a microemulsion (ME13). While the emission spectrum of C153 in heptane shows vibrational features, the corresponding one in water is devoid of any structure because of a stronger solute−solvent dipolar interaction. Also, the emission spectrum in water is noisy due to the very low solubility of C153 in water. Interestingly, the

peak frequency of the emission spectrum, ν_{em}, of C153 in hexanol (static dielectric constant $\varepsilon_0 \approx 12$) is red-shifted by about 3500 cm^{-1} relative to that in heptane ($\varepsilon_0 \approx 2$) but is blue-shifted by only about 600 cm^{-1} from that in water ($\varepsilon_0 \approx 80$). This indicates that a change from a nonpolar to moderately polar solvent stabilizes the excited state of a dipolar probe significantly. Further enhancement in ε_0, however, does not induce a linear increase in the stabilization energy as the solvent density does not differ appreciably.[58,59,64] The emission spectrum of C153 in microemulsion is red-shifted by ~400 cm^{-1} compared to that in hexanol, indicating an environment slightly more polar than bulk hexanol. When $\nu_{em}(10^3\ cm^{-1}) \approx 18.6$ is used as a value for the emission peak frequency of C153 in this microemulsion in a continuum model expression,[58,65] the average static dielectric constant is found to be ~16, which is close to that of cyclohexanone.[60] Interestingly, fluorescence studies of AOT/isooctane/water reverse micelles have also indicated a drastic reduction of the average polarity of water[29] and other nonaqueous solvents[64] upon confinement from the bulk values. Note also that the emission spectrum from the microemulsion is relatively broader, indicating the environmental inhomogeneity in the system. Therefore, the emission spectrum from the microemulsion is arising mostly from C153 dissolved in the polar solvent pool trapped inside the reverse micelle-like aggregation. The trapped solvent pool may also contain some amount of hexanol as well since the latter is partially miscible in water.

Because microscopic heterogeneity is rather generic for these complex systems, the fluorescence emission from the dissolved probe is expected to show significant excitation wavelength dependence. This is shown in Figure 2. Note that the full width at half-maxima (fwhm), shown in the upper panel, narrows by about 500 cm^{-1} as the excitation wavelength changes from 378 to 460 nm, whereas the emission peak frequency shows a red shift by about 1000 cm^{-1} in the same excitation wavelength range. This red shift together with the shrinking of the bandwidth of the emission spectrum clearly reflects the distribution of C153 in various solvent components (polar and nonpolar) as well as those in different layers in the solvent pool trapped inside the microemulsion droplets. The polarity of the trapped solvent pool affects the fluorescence emission of C153 in a manner similar to that in bulk polar solvents (red shift in the emission spectrum with simultaneous narrowing of the bandwidth as the solvent polarity increases);[60] the observed narrowing of the emission spectrum probably indicates that as the excitation wavelength becomes longer, the C153 population trapped in a relatively more "homogeneous" and polar environment is excited more selectively. If this is true, then the relative Stokes shift, $\Delta\Delta\nu = (\nu_{abs} - \nu_{em})_{polar} - (\nu_{abs} - \nu_{em})_{nonpolar}$[58–60] due to polar interaction alone should increase with the increase in the excitation wavelength. A near linearity of $\Delta\Delta\nu$ with λ_{exc} is obtained in the present study[66] (not shown here), which also reflects the spatial distribution of C153 molecules in these microemulsions. Note that a similar heterogeneous distribution of environment around a dissolved probe was also observed earlier in AOT/water reverse micelles[3,26] and ionic liquids.[67]

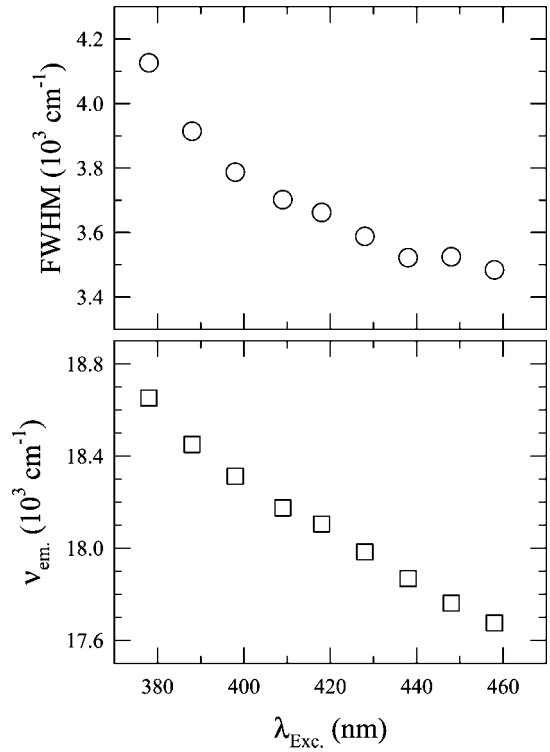

Figure 2. Excitation wavelength (λ_{exc}) dependence of the full width at half-maximum (fwhm) of the emission spectrum (upper panel) and emission peak frequency (lower panel) of C153 in a microemulsion (ME13) at a 0.830 weight fraction of SDS content. The narrowing of the fwhm with the increase in λ_{exc} indicates a more "homogeneous" environment being probed with larger λ_{exc} inside of a catanionic microemulsion droplet at a given composition. The emission peak frequency of C153 in the ME13 microemulsion shows a red shift as the excitation wavelength increases. Note the concomitant narrowing of the fluorescence emission spectrum with the red shift of the emission peak frequency. This correlation between the emission peak frequency and the emission bandwidth is similar to that from earlier studies where the emission of C153 in pure polar solvents showed simultaneous narrowing with the red shift as the polarity of the solvent increased. This indicates that the relative Stokes shift, $\Delta\Delta\nu = [\nu_{abs} - \nu_{em}]_{polar} - [\nu_{abs} - \nu_{em}]_{nonpolar}$, will also increase for this system as a function of λ_{exc}. This may be interpreted as a more polar region being probed with larger λ_{exc}. The error associated with the frequency values reported here is ±250 cm^{-1}.

3.2. Solubilization of *n*-Hexanol and Enzymatic Activity. The activity of an enzyme in a microemulsion is substantially influenced by the composition of the interface. Therefore, incorporation of alcohol molecules as the cosurfactant at the oil−water interface is likely to affect the enzyme activity inside the microemulsion droplets. Generally, alcohol molecules with more than four carbon atoms in its alkyl group are known to be a good cosurfactant, and hence, *n*-hexanol is a good cosurfactant for the catanionic microemulsion studied here.[68,69] The upper panel of Figure 3 demonstrates that with the increase of *n*-hexanol in the microemulsion at a fixed SDS/(SDS + DTAB) weight fraction and buffer content, the hydrodynamic diameter of the droplet increases. It is evident from this figure that the increase in *n*-hexanol leads to a swelling that increases the hydrodynamic diameter of the droplets. Interestingly, the enzymatic activity of horseradish peroxidase (HRP), shown in the same panel, also decreases as the droplet size increases upon addition of *n*-hexanol. Since the HRP activity in different *n*-alcohol−citrate buffer-saturated solutions is reported to be significantly lower,[45–47] the present results demonstrate that the HRP activity at the interface is strongly reduced by *n*-hexanol. The following reasons may be responsible for the weakening of the HRP activity at the interface. First, the denaturant property of *n*-hexanol molecules present at the interface is likely to reduce the activity of the enzyme. Second, there could be a structural transition[43] of the spherical (assumed) microemulsion droplets at a higher concentration of *n*-hexanol to aspherical nanostructures,where the confined fluid might not be able to optimally hydrate the enzyme for its activity.

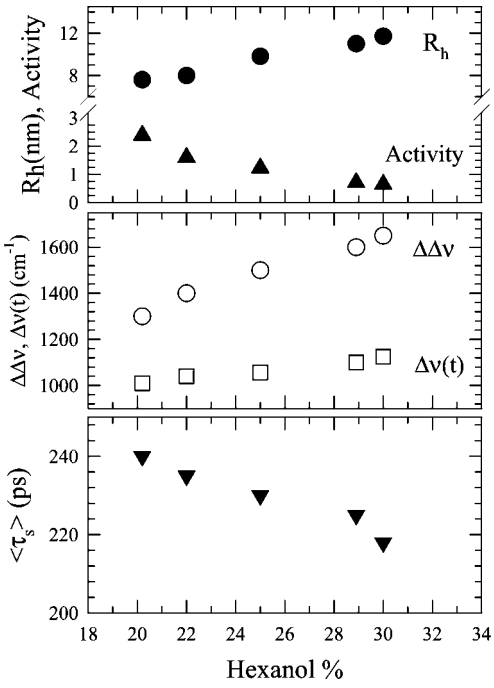

Figure 3. Variation of the hydrodynamic diameter, R_h, enzyme activity of horseradish peroxidase (Activity), relative Stokes shift, $\Delta\Delta\nu$, Stokes shift observed in our time-resolved experiments, $\Delta\nu(t) = \nu(0) - \nu(t)$, and average solvation time, $\langle\tau_s\rangle$, as a function of hexanol concentration for C153 in microemulsion at a 0.92 weight fraction of SDS and 22% (w/w) of buffer content. Note that at various hexanol concentrations, the hydrodynamic diameter (solid circle) and enzyme activity (solid triangle) are shown in the upper panel, the relative Stokes shift (open circle) and Stokes shift from time-resolved experiments (open squares) are shown in the middle panel, and the average solvation time is shown in the lower panel. The enzymatic activity data have been taken from ref 34.

3.3. Polarity of the Confined Fluid and Its Dynamics. As the polarity of a medium plays a crucial role in determining the reaction pathway as well as the products, one would like to know the average polarity of the polar solvent inside the pool of the microemulsion droplets. Also, since the polarity of a fluid and its structure determine the time scale of the environment reorganization around an excited solute, the study of solvation dynamics may supply useful information for correlating the medium dynamics with the enzymatic activity of HRP in the catanionic microemulsion. Solvation dynamics of laser-excited C153 dissolved in these microemulsions have been measured with a different hexanol content (20.2−30%, Table 1b). The time-dependent Stokes shifts, $\Delta\nu(t)$,[70] observed for these samples are shown as a function of hexanol content in the middle panel (open squares) of Figure 3. The relative Stokes shifts, $\Delta\Delta\nu$, obtained for these systems from the steady-state absorption and fluorescence emission measurements are also shown in the same panel. The magnitudes of both $\Delta\Delta\nu$ and $\Delta\nu(t)$ for these microemulsions indicate that the average dielectric constants of the confined environments of the microemulsion droplets are in the range of 10−20.[60] Note that the molecular dynamics simulations[51] and experimental studies[3,64] of AOT/water reverse micelles have also indicated a similar polarity of the confined water pool.

The decay of $S(t)$ in all of these systems is found to be a biexponential function of time. It is likely that fast components with time scales shorter than 15 ps might have been missed due to the limited time resolution employed in our experiments. We will come back to this point later. However, this limitation is not likely to affect the qualitative understanding of the average solvation time scales in these complex environments. The average solvation time, $\langle\tau_s\rangle$, obtained from the time-resolved measurements for these systems are shown as a function of *n*-hexanol content in the bottom panel of Figure 3. Note that the variation in $\langle\tau_s\rangle$ is small (within 220−240 ps) for the change in droplet diameter from 8 to 12 nm. A similar weak dependence of $\langle\tau_s\rangle$ on droplet size was observed earlier in quaternary microemulsions.[9,71] Since hexanol is miscible with dodecane, the solvation dynamics may derive a slow component from the preferential solvation of the excited probe. Such a study in binary mixtures of hexanol/isooctane reports $\langle\tau_s\rangle$ in the nanosecond range.[71] As dodecane is larger in size than isooctane, the average solvation time for a hexanol/dodecane binary mixtures is also expected to be at least in the same range. Therefore, the time scales (220−240 ps) are likely to be associated with solvation dynamics in these catanioinc micromulsions. However, even within this small range of diameter change, $\langle\tau_s\rangle$ shows a very small decrease. This is consistent with the current understanding of solvation dynamics in confined media, where solvent molecules are believed to be more mobile in a larger solvent pool.[1−29] Nevertheless, the average solvation time found for these systems is in the expected range for microemulsions,[2,3,7] and the dielectric constant of water decreases drastically upon confinement in the microemulsion droplet. Also, the tetrahedral hydrogen bonding network structure of water is partially destroyed in trapped water within the nanosized droplets. This, in turn, is likely to modify the bulk demixing behavior of water−hexanol mixtures.

The weak dependence of the average solvation time ($\langle\tau_s\rangle$) on the hexanol concentration may, however, arise due to the nondetection of the ultrafast dynamics of the confined polar pool in these microemulsions. It might be that nearly all of the initial fast energy relaxation via the collective solvent mode (small-amplitude motion of the hydrogen-bonded network in water) is missed due to the limited time resolution employed in our experiments, leaving only the diffusive dynamics at a relatively longer time to be detected. A recent study of polar solvation dynamics in quaternary microemulsions has indicated the presence of ultrafast dynamics on the time scale of ∼30 fs with a relatively large amplitude.[9] The solvation response measurements in lecithin vesicles[16] by using the three-pulse photon echo peak shift technique also reveals an ultrafast component with time scale in the range of 10−20 fs. Recently, vibrational echo and pump−probe measurements[26] have suggested that a significant portion (∼30−50%) of the total decay of the frequency−frequency correlation function for water confined in AOT/water reverse micelles is indeed ultrafast and deacys on a time scale in the range of 30−50 fs. This study[26] has also revealed a moderate dependence on the pool size of the time scales and amplitudes of the ultrafast components observed in the AOT/water reverse micelles. Note that these time scales are very similar to what has been observed in the polar solvation dynamics study of bulk water at ambient conditions.[72] Since water constitutes an important component (as the buffer) in all of the microemulsions studied, there is a definite possibility that we have missed completely the ultrafast dynamics that might have been present in these catanionic reverse micelles. The analyses by using the Fee−Maroncelli method[61] seems to suggest that the missing portion could be as large as 50% of the total decay of the solvent response function measured for all of the microemulsions considered here. Naturally therefore, the average solvation time ($\langle\tau_s\rangle$) shows a weak dependence or even insensitivity to the size of the microemulsion droplets.

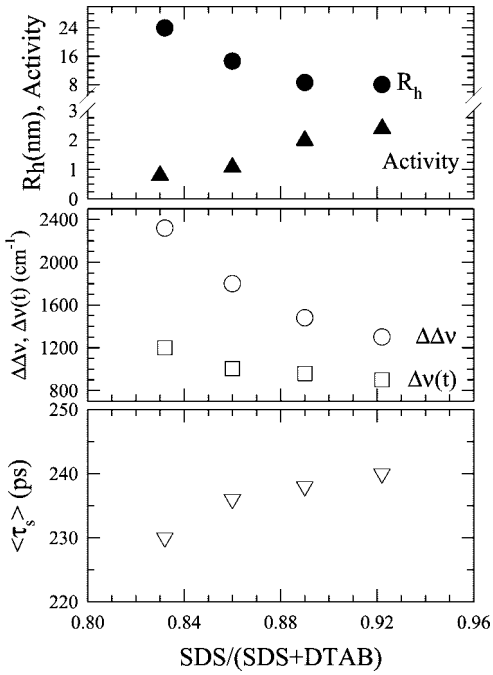

Figure 4. Effects of the SDS weight fraction (Table 1a) on the hydrodynamic diameter, R_h, enzyme activity of horseradish peroxidase (Activity), relative Stokes shift, $\Delta\Delta\nu$, Stokes shift observed in our time-resolved experiments, $\Delta\nu(t) = \nu(0) - \nu(t)$, and average solvation time, $\langle\tau_s\rangle$, for C153 in a microemulsion at 22.0 and 20.2% weight fractions of buffer and hexanol, respectively. The other representations remain the same as that in Figure 3. Enzymatic data are from ref 34. For details, see the text.

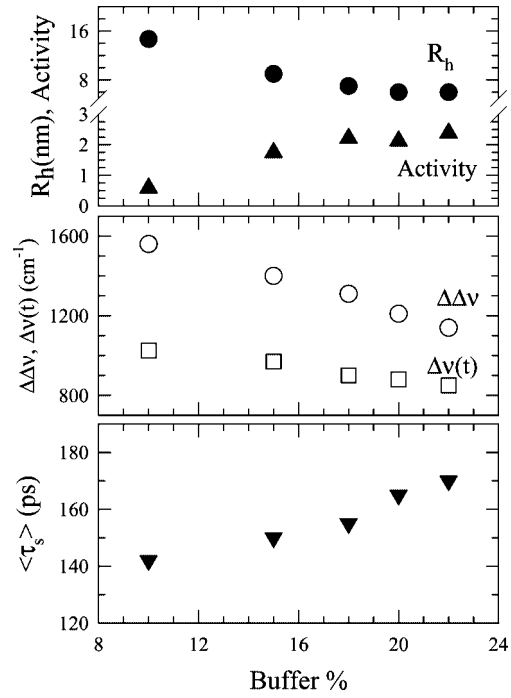

Figure 5. Effects of buffer composition (Table 1c) on the hydrodynamic diameter, R_h, enzyme activity of horseradish peroxidase (activity, ref 34), relative Stokes shift, $\Delta\Delta\nu$, Stokes shift observed in our time-resolved experiments, $\Delta\nu(t) = \nu(0) - \nu(t)$, and average solvation time, $\langle\tau_s\rangle$, for C153 in a microemulsion at 0.9221 and 20.2 weight fractions of SDS and buffer, respectively. The other representations remain the same as those in Figure 3.

3.4. Influence of the Surfactant and Buffer on the Droplet Size and Dynamics. We have varied the weight fraction of SDS [i.e., SDS/(SDS + DTAB)] from 0.830 to 0.9221% (Table 1a) to examine its effect on the HRP enzyme activity. The HRP activity has been found to increase with the increase in SDS content.[34] The effect of SDS on the droplet size is shown in the upper panel of Figure 4. Note that the dependence of the droplet size and its correlation with the HRP activity is similar to what has been found when the *n*-hexanol concentration was varied (activity inversely proportional to droplet size). Also note that the HRP activity is the maximum when the droplet size is the minimum (~8 nm in the present study). With the increase in SDS, the cosurfactant (*n*-hexanol in this case) should be gradually replaced by it in the interface. This would enhance the electrostatic attraction between the counter-charged surfactants, leading to a decrease in the total surface area. As a result, the percolation of *n*-hexanol into the confined solvent pool should also decrease, which, in turn, would enhance the activity of HRP. This is probably the reason for the increase in the HRP activity with the increase in the SDS content (filled triangles in the upper panel of Figure 4). The polarity of the solvent pools inside the microemulsion droplets has also been probed and presented in the middle panel of Figure 4. Clearly, $\Delta\Delta\nu$ and $\Delta\nu(t)$ are again similar in magnitude to those presented in Figure 3. The decrease in both of these quantities upon increasing the SDS content reflects the reduced pool size and correlates well with DLS results. The average solvation time, $\langle\tau_s\rangle$, presented in the bottom panel of Figure 4, shows a small increase with the increase in SDS content. It is interesting, however, that the average solvation time changes very little upon increasing the SDS fraction from 0.83 to 0.92, while the hydrodynamic diameter reduces by a factor of ~3 in the same SDS range (upper panel). Since successive addition of SDS increasingly ejects out *n*-hexanol from the interstitial spaces and brings the other surfactant molecules with counter charge closer through the electrostatic attraction, the droplet size becomes smaller. Here also, the estimated missing component of the ultrafast dynamics ranges between 45 and 55%. This may be one of the reasons for the observed weak dependence of the average solvation time on the SDS fraction.

The effects of buffer (water) on the droplet size and solvation dynamics are shown in Figure 5. The enzyme activity is known to show the maximum activity when it is properly hydrated.[73–75] Since the increase in buffer concentration is in line with an increased water content of the medium, the enzyme activity is expected to increase. This is indeed the result, which is shown in the upper panel of Figure 5. However, the droplet size decreases by approximately a factor of 2 upon increasing the buffer from 10 to 15% and then becomes almost insensitive to further increase in buffer concentration. As the buffer content increases, the relative amount of hexanol at the interface decreases, even though the critical micellar concentrations for all of the surfactants in the solution are maintained. The dilution of the cosurfactant (*n*-hexanol) actually decreases its localization into the reverse micelle film. This is responsible for the initial decrease in the hydrodynamic diameter of the droplets. The decrease in the *n*-hexanol concentration assists HRP activity by both reducing the probability of alcohol poisoning of the enzyme and also supplying a larger number of water molecules for the enzyme to hydrate properly.

The buffer concentration dependencies of the relative Stokes shift, $\Delta\Delta\nu$, and the average solvation time, $\langle\tau_s\rangle$, are shown, respectively, in the middle and bottom panels of Figure 5. As expected, the magnitude of $\Delta\Delta\nu$ decreases as the droplet size is reduced. The time-dependent Stokes shift, $\Delta\nu(t)$, also shows a similar behavior. The magnitudes of $\Delta\Delta\nu$ and $\Delta\nu(t)$ again

TABLE 2: Anisotropy Decay Parameters for C153 in Microemulsions for Extreme Compositions for SDS, Hexanol, and Buffer Excited at 409 nm along with the Corresponding Hydrodynamic Diameter (R_h) (compositions of the microemulsions mentioned in Table *1*)

microemulsion samples	R_h (nm)	a_1	$\tau_{1\,(ps)}$	a_2	$\tau_{2\,(ps)}$	$\langle\tau_r\rangle$ (ps)
ME13	24	0.70	25	0.30	447	152
ME10	8	0.66	26	0.34	348	135
ME17	12	0.66	28	0.34	419	161
ME21	16	0.67	29	0.33	389	148

suggest that the average polarity (in terms of ε_0) inside these catanionic microemulsions ranges between 10 and 20. The amplitude of the missing component of the ultrafast dynamics is estimated to be in the range of 50−60%. As in the earlier cases, this may be the reason for the observed weak dependence of the average solvation time on the buffer concentration and, hence, on the size of the microemulsion droplets.

3.5. Solute Dynamics: Time-Resolved Fluorescence Anisotropy Study. While the study of the solvation dynamics in these complex environments provided information about solvent motions and their reorganization around a laser-excited solute, the coupling between the solute's rotational motion and that of the solvent molecules could be probed by investigating the time-resolved fluorescence anisotropy of the same excited solute molecule. The time-dependent fluorescence anisotropy decay of C153 in these catanionic microemulsions has been measured at the emission peak (∼535 nm) for different microemulsions. As already mentioned, the decays are found to be biexponential functions of time, giving rise to two rotational time constants, τ_1 and τ_2, for these microemulsions. Quite understandably, the short time constant, which is associated with the rotational motion of the dissolved probe (C153), should become shorter as the droplet size increases and the environment becomes less rigid. The long one, on the other hand, represents the global motion of the droplet and, therefore, should become longer as the droplet size increases. The values of the decay parameters are given in Table 2 for two terminal compositions for each series summarized in Table 1.

Note that in these systems, the anisotropy decay associates with a fast component, τ_1, of ∼30 ps (∼70%) and a slow component, τ_2, of ∼400 ps (∼30%). These well-separated time scales are indicative of two types of rotational motions involving C153, which are decoupled from each other. This is the typical behavior of our fluorescence anisotropy study for catanionic microemulsions at all compositions, which were seen earlier in reverse micelles[2,3] and also in quaternary microemulisons.[71] The average rotational correlation time,$\langle\tau_r\rangle$, has been determined for all of these catanionic microemulsions and is presented in Figure 6. The upper panel of Figure 6 indicates that $\langle\tau_r\rangle$ increases as the *n*-hexanol concentration increases. We have already seen (Figure 3) that the hydrodynamic diameter of the droplets increases with the *n*-hexanol concentration. Therefore, the fluorescence anisotropy results for these microemulsions correlate well with the DLS results. However, $\langle\tau_r\rangle$ does not show a linear increase with *n*-hexanol concentration as observed for the droplet diameter. This is because the swelling of the droplet affects the two time constants in a manner opposite to each other. As expected, the short time constant dominates at small droplet size, whereas the longer time constant dictates the magnitude of $\langle\tau_r\rangle$ at larger droplet diameters. The variation of $\langle\tau_r\rangle$ with SDS concentration and buffer percentage in the microemulsions is also shown, respectively, in the middle and bottom panels of Figure 6. The average rotational correlation

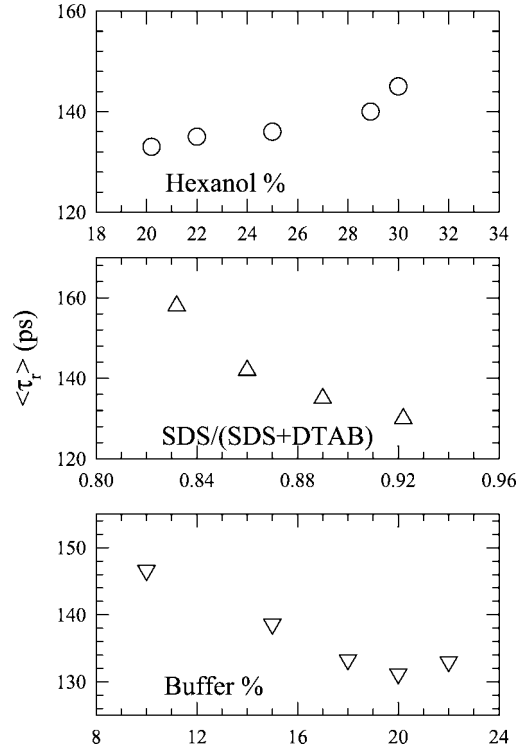

Figure 6. Upper panel: Hexanol composition (Table 1b) dependence of the average rotational time, $\langle\tau_r\rangle$, of C153 in microemulsions at a 0.92 weight fraction of SDS. Middle panel: Variation of $\langle\tau_r\rangle$ for C153 with SDS weight fraction at a 22.0% weight fraction of buffer. Lower panel: Dependence of $\langle\tau_r\rangle$ on buffer concentration (in percentage) in a microemulsion at a 0.9221 weight fraction of SDS. Note that in all cases, the anisotropy decay has been found to be biexponential with time, and $\langle\tau_r\rangle$ has been obtained by using the formula as discussed in the text.

times for these systems also correlate well with the DLS data. Note here that while the longest $\langle\tau_r\rangle$ corresponds with the lowest HRP activity and the smallest $\langle\tau_s\rangle$ for microemulsions obtained by varying the hexanol concentration, the maximum activity and the largest $\langle\tau_s\rangle$ occurs at an SDS fraction and buffer percentage where $\langle\tau_r\rangle$ is the lowest. This correlation between the enzyme activity and the average rotational and solvation times probably indicates that the enzyme activity is related to the slow dynamical modes of the medium. This is, however, in contrast to what has been observed for protein functionality in bulk water, where slowing down of the hydration dynamics has led to the suppression of enzyme activity.[76]

Another feature to note in Figure 6 is that the average rotational times for C153 in all of these microemulsions fall in the range of 120−160 ps, where the underlying anisotropy decays are biexponential in time. Time-resolved anisotropy studies of C153 in bulk polar solvents have shown that anisotropy decays are generally nonexponential and possess a fast component with a time constant of ∼20 ps for solvents with values of ε_0 in the range of 10− 20 and a longer time constant in the range of 100−200 ps (particularly for a few medium-sized alcohols).[63] The representative data in Table 2 also indicate the presence of fast components with similar time constants for C153 in microemulsions at different compositions. However, the fast time constant remains insensitive to the size of the microemulsions. A similar insensitivity to droplet size was observed earlier with a different dipolar probe in quaternary microemulsions.[71] As analyzed for average solvation time, this may also arise due to missing a component in $r(t)$ that is faster than our detection limit. The long time constant scales ap-

proximately with the size of the hydrodynamic diameter of the microemulsions.[77] Therefore, the average rotational correlation times are most likely those of C153 trapped inside of the microemulsions.

4. Conclusions

Enzymatic activity studies are a valuable tool to investigate local structures and compositions in confined media. However, these studies are not detailed enough to reveal local polarities and dynamics of the nanodroplets in the highly complex catanionic SDS/DTAB reverse microemulsion systems. In the present work, we are able to generate some understanding of the restricted enviroment/nanoenvironment of catanioinc reverse micelles that correlates with the previous results of HRP activity.[34] It is found that the activity of HRP becomes the maximum when the dynamical modes of the environment becomes the slowest. We believe that *n*-hexanol increases the interfacial fluidity of the microemulsion, hence its percolation. The other experimental findings also support this model along with the enzymatic activity study. Therefore, these systems can be used to get controlled enzyme activity, as we can monitor the internal environment by changing the fluidity. As a result, we think that we can now specifically design useful media for organic synthesis reactions, as the polarity of the core pseudophase can be externally monitored. Our systems contain a cationic surfactant (DTAB), which normally has an inhibition influence on the enzyme activity. However, the cationic−anionic interaction suppresses this inhibition effect, which also suggests that the DTAB molecules are not free in these systems but are located in the interfacial film of the microemulsions.

Further investigation with a sharper time resolution is required to understand the origin of the observed insensitivity of the average solvation and rotational times to the microemulsion droplet size. The missing component of the ultrafast solvent relaxation is estimated to be about 50% in these microemulsions for all of the compositions studied here. The time scales for this missing component need to be investigated in order to better understand the origin of the ultrafast time scales and their possible roles in determining the activity of the enzyme in these restricted environments. The time scale and amplitude of the initial part of the polar solvent energy relaxation in the quaternary microemulsions (33 fs)[9] and in lecithin vesicles (14 fs)[16] together with those obtained by vibrational echo measurements in AOT/water reverse micelles[26] render the study of solvation dynamics in these catanionic reverse micelles even more intriguing. At a similar droplet size, a comparison between the time scales observed in the present study, those reported for quaternary microemulsions, and those in AOT/water reverse micelles[2,3] seems to suggest that, dynamically, the solvent pool inside the quaternary microemulsions and AOT/water reverse micelles are, respectively, the fastest and slowest, whereas the catanionic pool stays in between. This may be due to the different nature of interactions of water molecules with the surfactant and surfactant mixtures constituting the microemulsions. Vibrational echo experiments[25,26] could be employed to investigate the difference in the nature of interactions between water molecules and surfactants, particularly near the inner surface of the microemulsions. Computer simulation studies of structure and dynamics of water molecules in mixed surfactant systems would be helpful to understand the difference in interaction that may lead to a different dynamical behavior of the trapped environment. Also, an excitation wavelength dependence study of both solvation and rotational dynamics in the catanionic microemulsions may be very interesting. Simple chemical reactions such as intramolecular charge-transfer or isomerization reactions in these media could be studied in order to investigate the effects of slow medium dynamics. Some of the above studies are already in progress.[78]

Acknowledgment. R.B. and S.M. are thankful to the Directors, S. N. Bose National Centre for Basic Sciences, Kolkata, India, and the North−East Institute of Science & Technology, Jorhat, India, for support and encouragement. S.M. thanks DAAD, Germany, for an equipment grant. R.B. thanks CSIR, India, for partial financial assistance. The authors thank Ms. P. Ghoshal for help at the initial stage of this work. We thank anonymous reviewers for several valuable suggestions.

References and Notes

(1) Levinger, N. E. *Science* **2002**, *298*, 1722.
(2) Bhattacharyya, K. *Acc. Chem. Res.* **2003**, *36*, 95. and references therein.
(3) Ghosh, S.; Mandal, U.; Adhikari, A.; Dey, S.; Bhattacharyya, K. *Int. Rev. Phys. Chem.* **2007**, *26*, 421.
(4) Luisi, P. L., Straub, B. E., Eds., *Reverse Micelles: Biological and Technological Relevance to Amphiphilic Structures in Apolar Media*; Plenum: New York, 1984.
(5) De, T.; Maitra, A. *Adv. Colloid Interface Sci.* **1995**, *59*, 95.
(6) Baruah, B.; Roden, J. M.; Sedgwick, M.; Correa, N. M.; Crans, D. C.; Levinger, N. E. *J. Am. Chem. Soc.* **2006**, *128*, 12758.
(7) Willard, D. M.; Riter, R. E.; Levinger, N. E. *J. Am. Chem. Soc.* **1998**, *120*, 4151.
(8) Harpham, M. R.; Ladanyi, B.; Levinger, N. E. *J. Phys. Chem. B* **2005**, *109*, 16891.
(9) Corbeil, E. M.; Levinger, N. E. *Langmuir* **2003**, *19*, 7264.
(10) Correa, N. M.; Levinger, N. E. *J. Phys. Chem. B* **2006**, *110*, 13050.
(11) Rosenfeld, D. E.; Schmuttenmaer, C. A. *J. Phys. Chem. B* **2006**, *110*, 14309.
(12) Vanables, D. S.; Huang, K.; Schmuttenmaer, C. A. *J. Phys. Chem. B* **2001**, *105*, 9132.
(13) Boyd, J. E.; Briskman, A.; Sayes, C. M.; Mittelman, D. A.; Colvin, V. *J. Phys. Chem. B* **2002**, *106*, 6346.
(14) Boyd, J. E.; Briskman, A.; Colvin, V. L.; Mittleman, D. M. *Phys. Rev. Lett.* **2001**, *87*, 147401/1.
(15) Zhong, Q.; Steinburst, D. A.; Carpenter, E. E.; Owrutsky, J. C. *Langmuir* **2002**, *18*, 7401.
(16) Bursing, H.; Ouw, S.; Kundu, P.; Vohringer, P. *Phys. Chem. Chem. Phys.* **2001**, *3*, 2378.
(17) Pileni, M. P., Ed. *Structure and Reactivity in Reverse Micelles*; Elsevier: Amsterdam, The Netherlands, 1989; Vol. 65.
(18) Cho, C. H.; Chung, M.; Lee, J.; Nguyen, T.; Singh, S.; Vedamuthu, M.; Yao, S.; Zhu, S. B.; Robinson, G. W. *J. Phys. Chem.* **1995**, *99*, 7806.
(19) Lundgren, J. S.; Heitz, M. P.; Bright, F. V. *Anal. Chem.* **1995**, *67*, 3775.
(20) Das, S.; Datta, A.; Bhattacharyya, K. *J. Phys. Chem. A* **1999**, *101*, 3299.
(21) Sarkar, N.; Das, K.; Datta, A.; Das, S.; Bhattacharyya, K. *J. Phys. Chem.* **1996**, *100*, 10523.
(22) Datta, A.; Mandal, D.; Pal, S. K.; Bhattacharyya, K. *J. Phys. Chem. B* **1997**, *101*, 10221.
(23) Riter, R. E.; Willard, D. M.; Levinger, N. E. *J. Phys. Chem. B* **1998**, *102*, 2705.
(24) Moilanen, D. E.; Levinger, N. E.; Spry, D. B.; Fayer, M. D. *J. Am. Chem. Soc.* **2007**, *129*, 14311.
(25) Tan, H.-S.; Piletic, I. R.; Fayer, M. D. *J. Chem. Phys.* **2005**, *122*, 174501.
(26) Piletic, I. R.; Tan, H.-S.; Fayer, M. D. *J. Phys. Chem. B* **2005**, *109*, 21273.
(27) Faeder, J.; Ladanyi, B. M. *J. Phys. Chem. B* **2001**, *105*, 11148.
(28) Faeder, J.; Ladanyi, B. M. *J. Phys. Chem. B* **2000**, *104*, 1033.
(29) Bhattacharyya, K.; Bagchi, B. *J. Phys. Chem. A* **2000**, *104*, 10603.
(30) Salaniwal, S.; Cui, S. T.; Cochran, H. D.; Cummings, P. T. *Langmuir* **2001**, *17*, 1773.
(31) Salaniwal, S.; Cui, S. T.; Cochran, H. D.; Cummings, P. T. *Langmuir* **2001**, *17*, 1784.
(32) Salaniwal, S.; Cui, S. T.; Cochran, H. D.; Cummings, P. T. *Langmuir* **1999**, *15*, 5188.
(33) Senapati, S.; Keiper, J. M.; DeSimone, J. M.; Wignall, G. D.; Melnichenko, Y. B.; Frielinghaus, H.; Berkowitz, M. L. *Langmuir* **2002**, *18*, 7371.
(34) Mahiuddin, S.; Renoncourt, A.; Bauduin, P.; Touraud, D.; Kunz, W. *Langmuir* **2005**, *21*, 5259.

(35) Shi, H. T.; Qi, L. M.; Ma, J. M.; Cheng, H. M. *Chem. Commun.* **2002**, 1704.
(36) Shi, H. T.; Qi, L. M.; Ma, J. M.; Cheng, H. M.; Zhu, B. Y. *Adv. Mater.* **2003**, *15*, 1647.
(37) Shi, H. T.; Wang, X. H.; Zhao, N. N.; Qi, L. M.; Ma, J. M. *J. Phys. Chem. B* **2006**, *110*, 748.
(38) López-Quinteta, M. A.; Tojo, C.; Blanco, M. C.; García-Rio, L.; Leis, *Curr. Opin. Colloid Interface Sci.* **2004**, *9*, 264.
(39) Khan, A.; Marques, E. In *Specialist Surfactant*; Robb, I., Ed.; Blanckie Academic and Professional: London, 1997; Chapter 3 and references therein.
(40) Jokela, P.; Jonsson, B.; Khan, A. *J. Phys. Chem.* **1987**, *91*, 3291.
(41) Li, X.; Ueda, K.; Kunieda, H. *Langmuir* **1999**, *15*, 7973.
(42) Li, X.; Kunieda, H. *Curr. Opin. Colloid Interface Sci.* **2003**, *8*, 327. and references therein.
(43) Abécassis, B.; Testard, F.; Arleth, L.; Hansen; S.; Grillo, I.; Zemb, T. *Langmuir,* **2006**, *22*, 8017.
(44) Pinna, C.; Bauduin, P.; Touraud, D.; Monduzzi, M.; Ninham, W. B.; Kunz, W. *J. Phys. Chem. B* **2005**, *109*, 16511.
(45) Bauduin, P.; Touraud, D.; Kunz, W.; Savelli, M. P.; Ninham, B. W. *J. Colloid Interface Sci.* **2005**, *292*, 244.
(46) Cinelli, S.; Onori, G.; Santucci, A. *Colloids Surf., A* **1999**, *160*, 3.
(47) Shimizu, S.; Shimizu, K. *J. Am. Chem. Soc.* **1999**, *121*, 2387.
(48) Pal, S. K.; Peon, J.; Bagchi, B.; Zewail, A. H. *J. Phys. Chem. B* **2002**, *106*, 12376.
(49) Pal, S. K.; Zewail, A. H. *Chem. Rev.* **1999**, *104*, 2099.
(50) Halder, M.; Mukherjee, P.; Bose, S.; Hargrove, M. S.; Song, X.; Petrich, J. W. *J. Chem. Phys.* **2007**, *127*, 055101.
(51) Balasubramanian, S.; Bagchi, B. *J. Phys. Chem. B* **2001**, *105*, 12529.
(52) Senapati, S.; Chandra, A. *J. Phys. Chem. B* **2001**, *105*, 5106.
(53) Nandi, N.; Bagchi, B. *J. Phys. Chem. B* **1997**, *101*, 10954.
(54) Nandi, N.; Bhattacharyya, K.; Bagchi, B. *Chem. Rev.* **2000**, *100*, 2013.
(55) Prakash, M. K.; Marcus, R. A. *J. Phys. Chem. B* **2008**, *112*, 399.
(56) Abécassis, B.; Testard, F.; Arleth, L.; Hansen, S.; Grillo, I.; Zemb, T. *Langmuir* **2007**, *23*, 9983.
(57) Das, T. K.; Mazumdar, S. *Eur. J. Biochem.* **1995**, *227*, 823.
(58) Biswas, R.; Lewis, J. E.; Maroncelli, M. *Chem. Phys. Lett.* **1999**, *310*, 485.
(59) Lewis, J. E.; Biswas, R.; Robinson, A. G.; Maroncelli, M. *J. Phys. Chem. B.* **2001**, *105*, 3306.
(60) Horng, M. L.; Gardecki, J. A.; Papazyan, A.; Maroncelli, M. *J. Phys. Chem.* **1995**, *99*, 17311.
(61) Fee, R. S.; Maroncelli, M. *Chem. Phys.* **1994**, *183*, 235.
(62) Sen, S.; Dutta, P.; Sukul, D.; Bhattacharyya, K. *J. Phys. Chem. A* **2002**, *106*, 6017.
(63) Horng, M. L.; Gardecki, J. A.; Maroncelli, M. *J. Phys. Chem. A* **1997**, *101*, 1030.
(64) Biswas, R. (Unpublished data).
(65) The following correlation is used to estimate the dielectric constant of ME13 from the emission frequency of C153: $\nu_{em}(10^3\ cm^{-1}) = 23.12 - 5.06[(\varepsilon_0 - 1)/(\varepsilon_0 + 2)] - 1.5[(n^2-1)/(n^2 + 2)]$, where refractive index (n) of the medium is assumed to be that of bulk water. For details, see refs 58 and 59.
(66) In order to calculate $\Delta\Delta\nu$ for a probe in a given medium, one needs the absorption and emission peak frequencies of that probe in a nonpolar bulk solvent and the absorption peak frequency of the probe dissolved in that medium. These values remain unchanged during the excitation wavelength dependence study of the emission peak frequency of the probe in that medium. Consequently, the linear dependence of emission peak frequency on excitation wavelength (λ_{exc}) is reflected in the correlation of $\Delta\Delta\nu$ versus $\lambda_{exc.}$,
(67) Jin, H.; Li, X.; Maroncelli, M. *J. Phys. Chem. B* **2007**, *111*, 13473.
(68) Clausse, M.; Nicolas-Morgantini, L.; Zradba, A.; TouraudD. Water−Ionic Surfactant−Alkanol−Hydrocarbon System: Influence of Certain Constitution and Composition Parameters upon the Realm of Existence and Transport Properties of Microemulsion Type Media. *Surfactant Science Series 24 (Microemulsion Systems)*; 1987; pp 15−66.
(69) Ray, S.; Moulik, S. P. *J. Colloid Interface Sci.* **1995**, *173*, 28.
(70) The time-dependent Stokes shift is calculated as follows: $\Delta\nu(t) = \nu_{t=0}^{obs} - \nu_{t=\infty}$. That is, the difference between the emission peak frequencies at $t = 0$, as observed in our experiment, and that after the solvent relaxation is complete.
(71) Hazra, P.; Chakrabarti, D.; Chakraborty, A.; Sarkar, N. *Chem. Phys. Lett.* **2003**, *382*, 71.
(72) Jimenez, R.; Fleming, G. R.; Kumar, P. V.; Maroncelli, M. *Nature* **1994**, *369*, 471.
(73) Avramiotis, A.; Papadimitriou, V.; Cazianis, C. T.; Xenakis, A. *Colloids Surf., A* **1998**, *144*, 295.
(74) Rees, G. D.; Robinson, B. H. *Biotechnol. Bioeng.* **1995**, *45*, 344.
(75) Ayala, G.; Mendoza-Hernandez, G. *Biochem. Int.* **1990**, *22*, 717.
(76) Pal, S. K.; Peon, J.; Zewail, A. H. *Proc. Natl. Acad. Sci. U.S.A.* **2002**, *99*, 15297.
(77) As the compositions of the microemulsions are different and hence the extent of solute−medium coupling differs, the scatters in the data (between ME17 and ME21) are expected.
(78) Biswas, R.; Mahiuddin, S. K. Unpublished data.

JP711368P